Effects of mould wear on hydrophobic polymer surfaces replicated using plasma-treated and laser-textured stainless steel inserts

Romano, Jean-Michel; Sarasa, Jorge; Concheso, Carlos ; Gulcur, Mert; Dashtbozorg, Behnam; Garcia Giron, Antonio; Penchev, Pavel; Dong, Hanshan; Whiteside, Ben ; Dimov, Stefan

DOI:
10.1080/17515831.2020.1785234

Effects of mould wear on hydrophobic polymer surfaces replicated using plasma treated and laser-textured stainless steel inserts

Jean-Michel Romano (1)*, Jorge Fantova Sarasa (2), Carlos Concheso (2), Mert Gulcur (3), Behnam Dashtbozorg (4), Antonio Garcia-Giron (1), Pavel Penchev (1), Hanshan Dong (4), Ben R. Whiteside (3), Stefan Dimov (1)

(1) School of Engineering, University of Birmingham, Edgbaston, Birmingham B15 2TT, UK

(2) Center for Corporate Technology and Innovation Spain, BSH Electrodomésticos España, S.A., 50016 Zaragoza, Spain

(3) Centre for Polymer Micro & Nano Technology, Faculty of Engineering and Informatics, School of Engineering, University of Bradford, Bradford BD7 1DJ, UK

(4) School of Metallurgy and Materials, University of Birmingham, Edgbaston, Birmingham B15 2TT, UK

* Contact: jean-michel.romano@gadz.org

Abstract

The mass production of polymeric parts with functional surfaces requires economically viable manufacturing routes. Injection moulding is a very attractive option however wear and surface damage can be detrimental to the lifespan of replication masters. In this research, the replication of superhydrophobic surfaces is investigated by employing a process chain that integrates surface hardening, laser texturing and injection moulding. Austenitic stainless steel inserts were hardened by low temperature plasma carburising and three different micro and nano scale surface textures were laser fabricated, i.e. submicron triangular Laser-Induced Periodic Surface Structures (LIPSS), micro grooves and Lotus-leaf like topographies. Then, a commonly available talc-loaded polypropylene was used to produce 5000 replicas to investigate the evolution of surface textures on both inserts and replicas together with their functional response. Any wear or surface damage progressively built up on the inserts during the injection moulding process had a clear impact on surface roughness and peak-to-peak topographies of the replicas. In general, the polymer replicas produced with the carburised inserts retained the wetting properties of their textured surfaces for longer periods compared with those produced with untreated replication masters.

Graphical abstract

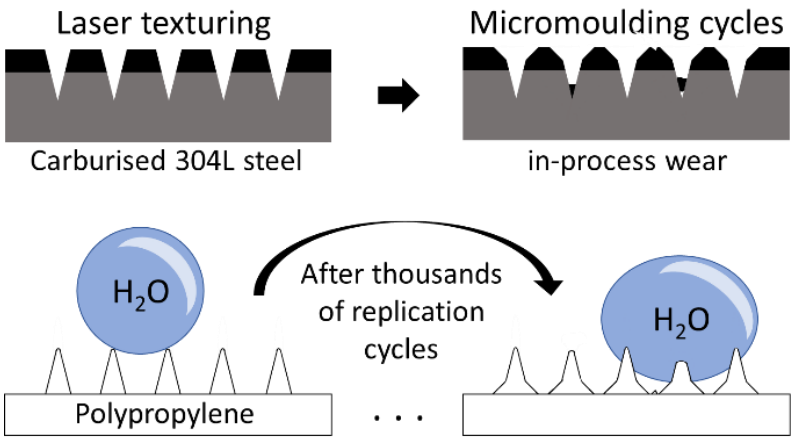

Keywords: wear, injection moulding, plasma surface alloying, laser texturing, wettability.

Word count:

Abstract: 183.

Article: 4734.

1. Introduction

The fabrication of products that incorporate surfaces with tailored wetting properties has attracted significant interest recently[1–3]. Inspired by water-repellent surfaces observed in nature, surface structures mimicking the Lotus-leaf[4], Rose petal[5] or Springtail cuticle[6,7] effects, among others, have been studied. An analytical description of wetting regimes was originally proposed by Wenzel[8] and Cassi-Baxter[9] and then used by many researchers to explain the response of various micro and nano scale structured/textured surfaces[10–13]. One of the technologies widely used to fabricate multi scale surface structures is ultra-short pulsed laser processing. In particular, the technology can be applied to produce Laser-Induced Periodic Surface Structures (LIPSS)[14,15] with superhydrophobic properties on metals[2,4,5,16–19] or polymers by direct laser writing[20,21] or by replication[22–24].

As a result of its cost-effectiveness, injection moulding has become a very attractive replication technology for the mass production of polymer components[25]. One of the polymers widely used to produce engineering parts is polypropylene, which has found industrial applications in automotive, aerospace and home appliances products as a result of its desirable mechanical and thermal properties[26]. In some cases, polymeric parts are reinforced by adding glass fibers in the blend. However, this comes in expense of increased mould wear and a reduced tool lifespan[25]. In other cases, fillers are added to the blend to reduce the material cost[26], but their effect on the mould lifespan is still to be assessed.

This research investigates the durability of stainless steel mould inserts used to produce talc-loaded polypropylene parts with hydrophobic surface properties. Especially, the surface functionality of replicas can be directly impacted as a result of any damage on injection moulds[27–29]. Therefore, material properties of replication masters, e.g. wear and corrosion resistance, become critical considerations[25,30]. Surface treatments, such as DLC coatings[31] or low temperature plasma treatments[32] can potentially be used to extend the lifespan of moulds by improving their wear, damage and corrosion resistance. To investigate the benefit of surface hardening, part of the inserts was carburised using a low temperature plasma treatment. Different surface textures were laser-fabricated on the mould inserts, with surface features in the range from several 100 nm to several 10s of microns. The evolution of surface damage to the mould with the increase of moulding cycles, up to 5000 shots, have been studied and discussed together with the respective wetting properties of the replicas.

2. Materials and methods

The process chain used in this research to produce polymeric parts with textured surfaces is presented in Fig. 1. The manufacturing route employed includes: i) machining of metallic inserts to the dimensions of the moulding cavity; ii) surface hardening through plasma carburisation; iii) fabrication of micro and nano scale surface structures using an ultra short pulsed laser; and finally, iv) the replication of the surface textures by injection moulding. In this section, these process stages together with the used characterisation techniques are described.

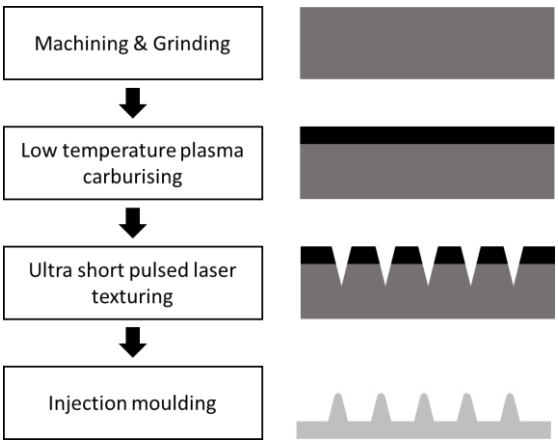

Figure 1. The process chain used in this research to produce polymer parts with textured surfaces.

2.1 Low temperature plasma carburising

Feasibility trials were conducted to determine if plasma carburasing could be applied after the laser texturing. They showed that applying this plasma treatment after the laser processing led to inhomogeneous diffusion of carbon in the sub surface and also to some modification of surface structures. Therefore, low temperature plasma carburising was perform only before the laser texturing operations.

First, the inserts were machined from 304L grade austenitic stainless steel to the dimensions of the moulding cavity, in particular a rectangular plate with dimensions of 60 mm x 40 mm. A surface alloying plasma treatment was utilised to diffuse carbon into the surfaces of the inserts. Since surface oxides can act as a dense barrier to plasma treatment, samples were freshly grounded down to #1200 grit size prior to plasma treatments. Additionally, samples were also ultrasonically cleaned using Teepol and acetone in order to remove any dust, grease or contaminants on surfaces.

The inserts were then DC plasma carburised (DC Klockner Ionon 40 kVA plasma furnace) in a working gas mixture of 98.5% H_2 : 1.5% CH_4 at a pressure of 3 mbars (see Fig. 2a). The samples were treated at 400°C for 30 h. Following this treatment, the inserts were gently polished using 1 µm diamond suspension in order to remove any loose sputtered material left over from the treatment.

2.2 Laser texturing

The treated stainless steel inserts were laser textured using a circular-polarised ultra-short pulsed laser (Amplitude Systemes Satsuma) with a wavelength of 1032 nm, 310 fs pulse duration and a repetition rate of 250 kHz. The beam delivery system used in this research is illustrated in Fig. 2b. In particular, a 100 mm focal length telecentric lens (QiOptiq LINOS) is integrated to focus the beam to a spot size of ~ 35 µm diameter at $1/e^2$ while a scan head (Newson RTA A2G) was utilised to steer the beam over the insert surface.

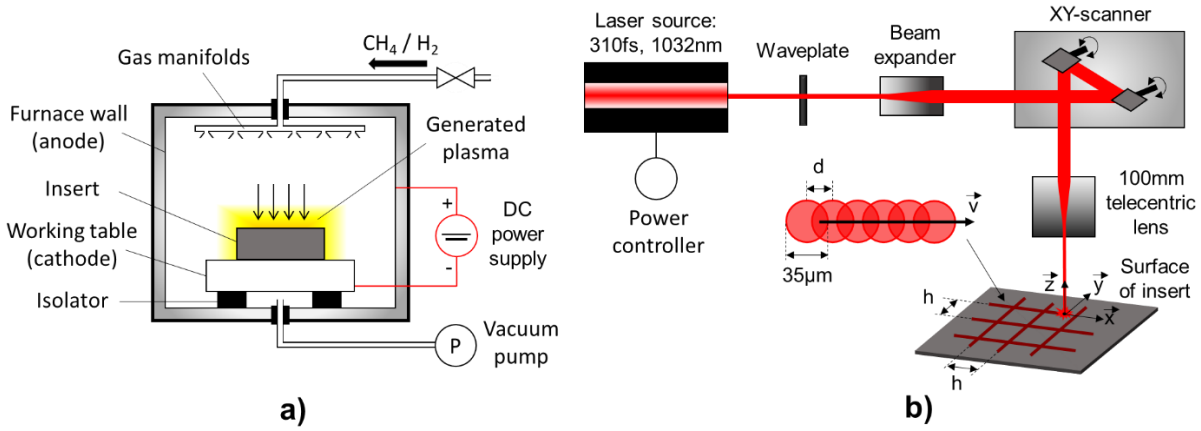

Figure 2. Diagrams depicting the plasma carburising and laser texturing setups used in the research, i.e. a) DC plasma carburising at 400°C in a gas pressure of 3 mbars; b) ultra-short laser processing in the near-infrared regime with beam spot of ~ 35 µm and surface scanning with a pulse-to-pulse distance d and hatch distance h.

Laser settings, i.e. the number of scans, fluence per pulse and hatch distance, were adjusted for producing three different surface textures and they are shown in Table 1. For each texture, the same process settings were used both on as-received stainless steel (S) and plasma carburised plates (C). The first topography was produced by parallel scan lines with a spatial displacement of 100 µm. The second one, with Lotus-leaf like structures was made by intersecting perpendicular scan lines with spatial displacement equal to the laser spot size, i.e. 35 µm. The third texture was generated using a single scan of close parallel lines at low fluence per pulse, enabling the LIPSS formation.

Table 1: List of laser processing parameters

Topography Nr.	**Description**	**Number of scans** (-)	**Fluence per pulse** (mJ/cm^2)	**Hatch distance** h (µm)	**Pulse-to-pulse distance** d (µm)
S0 and C0	Untextured	-	-	-	-
S1 and C1	Grooves	100	950	100	2
S2 and C2	Lotus	1250	950	35	35
S3 and C3	LIPSS	1	92	2	2

Notes: S0 to S3 and C0 to C3 denote as received and plasma carburised inserts, respectively.

After the laser processing, the inserts were ultrasonically cleaned in ethanol for 15 minutes, rinsed and dried with compressed air.

2.3 Injection moulding of polymeric parts

The untextured and textured inserts were integrated into an injection moulding machine (Arburg Allrounder 170) which is schematically depicted in Fig. 3a. A polypropylene (PP) homopolymer compound containing 30 wt% talc-based mineral fillers (LyondellBasell Hostacom HKC 182L W92607) was selected due to its common use in producing polymer parts of home appliances and other engineering applications. The temperatures of the 3-zone extrusion screw and nozzle were set at 225, 230, 230 and 235 °C from the hopper to the nozzle respectively while the mould temperature was set at 80 °C. The heating profile was

chosen based on the material datasheets and preliminary trials. The ranges of other important process variables, i.e. the flow rate from 20 to 45 cm^3/s, injection pressure from 350 to 650 bar and holding pressure from 350 to 750 bar were identified by conducting moulding trials using the laser-textured insert S1 (see Table 2). During the preliminary trials, the injection moulding parameters were chosen to maximise the peak-to-peak height of replicated surface structures on the PP samples while monitoring the demoulding and ejection conditions and also for presence of flashes. The duration of one injection moulding cycle was ~ 30 s and its stages i.e. mould closure, injection, holding, cooling , mould opening and ejection of the plastic part, are depicted in Fig. 3b. No demoulding agents were used to preserve the surface chemistry and also to prevent altering the tribological contact.

The final polymer parts are denoted throughout the text with a prefix 'R' for replicas that is followed by the designation of the insert material and texture number.

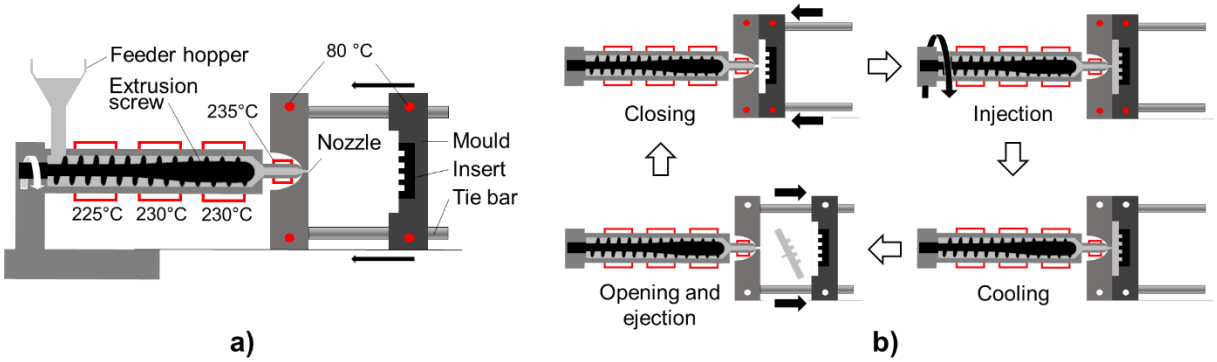

Figure 3. Schematic representations of injection moulding machine and moulding stages: a) the injection moulding setup used to fabricate the polypropylene parts; b) the stages of the injection moulding cycle.

Table 2: List of injection moulding parameters

Parameters	Units	Values
Screw temperature profile	°C	225, 230, 230
Nozzle temperature	°C	235
Mould temperature	°C	80
Injection flow rate	cm^3/s	42
Volume injected	cm^3	10 with 3 of cushion
Injection pressure	bar	450
Back pressure	bar	80
Holding pressure	bar	550, 500, 450, for 1, 3, 2 s respectively
Holding time	s	6
Cooling time	s	15
Full cycle time	s	~30

2.4 Material characterisation

The resulting carburised layer was characterised by employing destructive techniques. Composition-depth profiles were obtained using a glow-discharge optical emission spectrometer (Spectruma GDA 650HR). Microhardness was measured using a Mitutoyo MVK-H1 equipped with a Vickers indenter. Also, cross section characterisation was performed on the inserts following mirror-finish polishing and chemical etching (50% HCl : 25% HNO_3 : 25% H_20) to reveal the microstructure.

A focus variation microscope (Alicona G5, objective 50x) was used to measure the arithmetical mean (S_a) and maximum peak-to-valley (Δ_z) heights of the structured surfaces. The average values of nine measurements were used. Topographical datasets were acquired for areas of 800x800 μm^2 with vertical and lateral resolutions of 100 nm and 1.00 µm, respectively.

Also, the surfaces were inspected with a field emission gun scanning electron microscope (JEOL 7000F FEG-SEM). The polymer replicas were examined following a sputter coating of a thin gold layer and 10keV accelerating voltage was used to minimise any damage from the electron beam. The spatial periodicity of LIPSS were analysed using 2D Fast Fourier Transform (FFT) tools of the Gwyddion 2.51 software. The height of the LIPSS was measured using an atomic force microscope (Bruker Dimension 3100) equipped with tapping-mode probes (Nanosensors, PPP-Rt-NCHR).

Finally, the average values of static contact angles were obtained from nine measurements with an optical tensiometer (Biolin Scientific Attension Theta T2000-Basic+) by dispensing 6 µl of milli Q water in ambient conditions.

3. Results and discussion

3.1 Carburising and laser texturing of stainless steel inserts

The first step in producing the injection moulding inserts was the surface hardening of the 304L stainless steel workpieces. The composition-depth profiles of untreated and treated workpieces are provided in Fig. 4a-b. The profiles confirmed the oxygen content at the surface of untreated stainless steel samples, i.e. 9.0 wt%, while there were no traces of oxidation in the carburised ones. As a result of the plasma carburising treatment, the carbon content at the surface increased to 9.8 wt% compared with the 1.3 wt% of the untreated samples. The surface carbon content on untreated samples exhibits a sudden drop in concentrations, showing that they are very likely as a result of surface contaminations rather than carbon diffusion (see Fig. 4a). On the other hand, significant carbon content could still be seen in the composition profiles up to a depth of approximately 15 µm (see Fig. 4b). After the chemical etching of the cross section, a homogeneous layer could be clearly seen at the surface of the treated samples on top of underlying bulk filled with some inclusion holes (see Fig. 4c). Intrinsically, the dissolution of carbon atoms within the surface led to the expansion of the austenitic lattice[32]. This interstitial intercalation was associated with high compressive residual stresses[32], confirmed by an increase of the microhardness from 184 to 495 $HV_{0.05}$, i.e. for a load of 50 gf (see Fig. 4d). The load bearing capacity was examined, too, by increasing further the indentation load and it was found that there was still a 40% hardness enhancement even under a load of 500 gf.

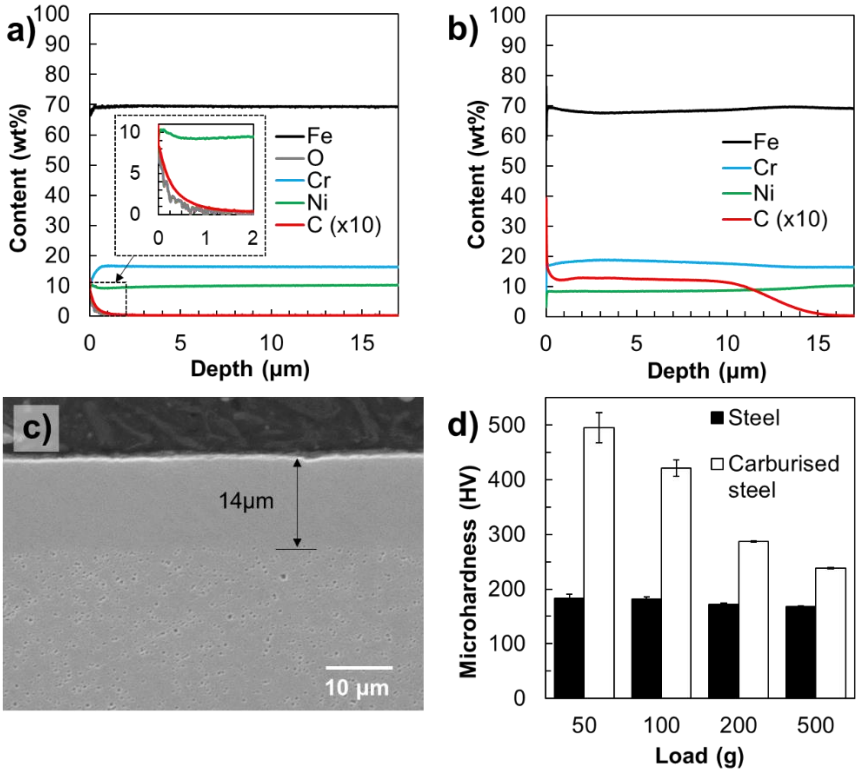

Figure 4. Composition-depth profiles of a) untreated (S0) and b) carburised (C0) inserts, c) a micrograph of the carbon expanded austenite layer and d) Vickers microhardness of untreated and carburised inserts.

The next step in producing the injection moulding inserts was surface texturing employing an ultrashort laser source. The three topographies that were investigated in this research are shown in Fig. 5. The laser processing parameters used to produce them are provided in Section 2.2. The first topography was parallel grooves with a 100 μm spacing that had a Gaussian-shaped profile with width and depth of approximately 39 and 65 μm, respectively (see Fig. 5a-b). The Lotus-leaf like structure included an array of holes with 37 μm diameter and approximately 60 μm depth (see Fig. 5c-d). The third topography consisted of Laser-Induced Periodic Surface Structures (LIPSS)[35,36] that covered homogeneously a 6 x 12 mm^2 area. An example of the submicron surface structures is provided in Fig. 5e-f.

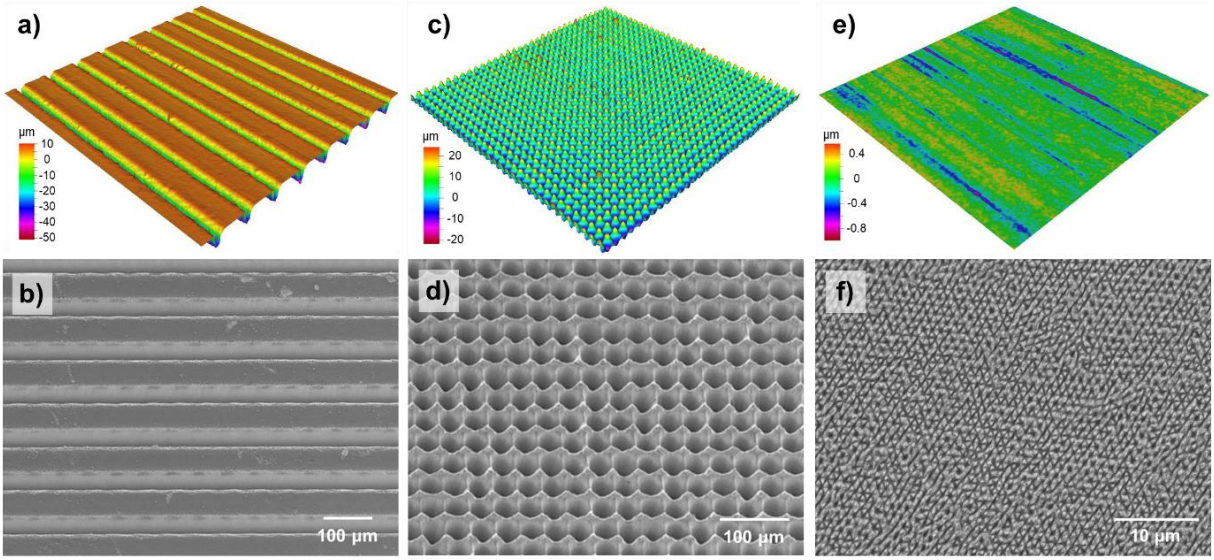

Figure 5. 3D views and SEM micrographs of the three investigated surface textures in this research, i.e. a-b) Grooves (S1), c-d) Lotus-leaf like (S2) and e-f) LIPSS (S3).

Note: The images in b) and d) are viewed at 45° angle.

The same process settings were used to texture both untreated and carburised stainless steel inserts and there were no significant differences in resulting topographies (see Fig. 6). In particular, the fabricated grooves (see Fig. 6a-b) and holes (see Fig. 6c-d) of the first two textures had similar depths and widths/diameters. Ultrashort laser processing with a polarised beam can simultaneously result in the creation of micro-scale features covered with LIPSS or some roughness[5]. In this research, submicron ripples covered the grooves and Lotus-leaf like textures and thus dual-scale surface structures were produced while the ablated material and nanoparticles were deposited around the processed areas[18]. A follow up ultrasonic cleaning did not allow the redeposited material and particles to be detached and removed and they could be clearly seen along the grooves (see Fig. 6a-b) and around the holes on unprocessed areas (see Fig. 6c-d).

Submicro-scale LIPSS textures both on treated and untreated inserts (C3 and S3, respectively) were triangular in shape and the FFTs indicated a clear hexagonal arrangement (see Fig. 6e-f). Ripple-like LIPSS fabricated on nitrided stainless steel by using femtosecond pulses was already reported[37] together with complex triangular LIPSS on stainless steel[38]. The spatial distance between the ripples was 10 to 20 % smaller into the nitrided layer compared with that on untreated samples and this was attributed to the compressive residual stresses in the plasma treated layer[37].In this research, the LIPSS generation on carburised stainless steel is demonstrated and the results have shown that this surface treatment made little difference on the LIPSS morphology (see Fig. 6e-f). In particular, the generated LIPSS on treated and untreated inserts had an average spatial periodicity of approximately 900 nm while the peak-to-valley distance varied between 80 and 200 nm.

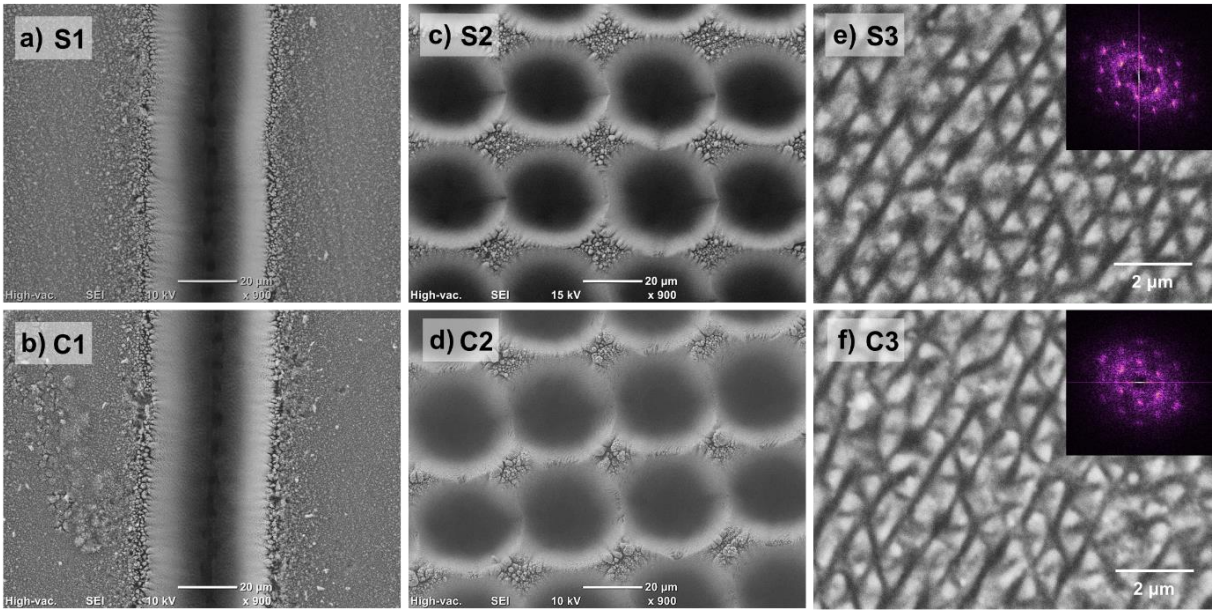

Figure 6. SEM micrographs of resulting topographies on untreated and carburised inserts, i.e.: a) S1, b) C1, c) S2, d) C2, e) S3, f) C3.

Notes: 1) the textures on untreated and carburised stainless steel are shown on top and bottom rows, respectively; 2) Grooves, Lotus-leaf like and LIPSS textures are shown from left to right; 3) the insets in e) and f) depict the respective 2D-FFTs of the S3 and C3 inserts.

Finally, it is worth mentioning that the carburised layer is inherently a metastable phase [32], i.e. an exposure to high temperatures could trigger the precipitation of carbides, and thus to alter dramatically the corrosion resistance. Laser texturing typically introduces a thermal load onto the surface with some associated negative side effects, especially when nanosecond laser pulses are employed [29,33]. Especially, a heat affected zone around the laser processed area can be observed, i.e. recasts and oxidation of the expanded layer, that leads to morphology, structure and mechanical properties modifications. By deploying femtosecond pulses, the laser-material interaction time is drastically shortened to a few picoseconds [34], and therefore the laser processing could be considered athermal [14]. This could be especially beneficial when processing metastable materials. Therefore, in this research, no thermal damage, such as cracking or subsurface precipitation, was observed after processing the carburised layer with femtosecond pulses with a repetition rate of 250 kHz. However, further investigations are required to characterize better the laser-matter interactions with the carburised layer.

3.2 Injection moulding of polymer replicas

The laser-textured inserts were mounted into the injection moulding modular tool and polymer replicas were produced with the process settings described in Section 2.3. The replicas of grooves and Lotus-leaf like textures were protruding structures with height of approximately 35 µm as shown in Figs 7a and 7b. The generation of textures with higher aspect ratios were attempted, too, and heights up to 48 µm were achieved, however, the demoulding performance was drastically reduced, i.e. the replicas could not be readily released from the inserts. Therefore, it was more appropriate in the context of this research to use textures with a lower aspect ratios and thus to achieve a replication efficiency of at least 55%.

Both micro- and submicron textures, especially with dual and single scales' features, were replicated simultaneously. For instance, the base and the walls of the micro features replicated from the grooves onto the inserts were covered with LIPSS, while their tops were smooth (see Fig. 7a). Similarly, denser surface topographies were produced with the Lotus-leaf like

textured inserts and again LIPSS were observed around the resulting protrusions (see Fig. 7b). The triangular LIPSS were also successfully replicated, with the resulting textures being negative copies in a clear hexagonal arrangement (see Fig. 7c). The peak-to-valley heights of the replicated submicron features were in the range of 40 to 140 nm while the replication efficiency was higher (up to 70-80%).

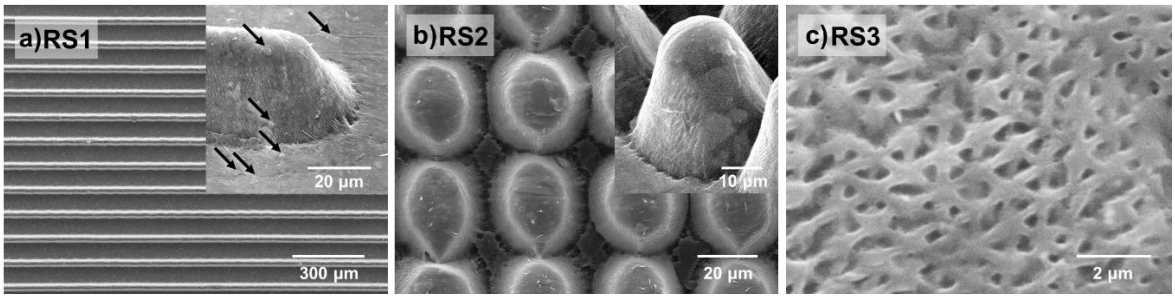

Figure 7. Top view SEM micrographs of the textured PP replicas: a) Grooves (RS1), b) Lotus-leaf like (RS2) and c) LIPSS (RS3).

Notes: The images in the insets a) and b) were viewed at 45° angle and the black arrows point out some mineral fillers.

The mineral fillers are visible on the planar surface of the moulded parts and also on the replicated surface structures (see insets in Fig. 7a-b). The filler-matrix interface was analysed by cryogenically fracturing the PP parts in liquid nitrogen. The layers of fillers and platelet talc particles with sizes from half a micron up to dozens of microns could be seen in the polymer matrix. The fillers had a random-in-plane alignment in the polymer bulk and an orientation parallel to the flow direction in the replicas' skin layers due to combination of elongation forces and shear flow around the melt front[39,40], as shown in Fig. 8a. Also, the replicated groove-structures, depicted in Fig. 8b, illustrate how the polymer fills the cavities. The talc platelets inside the surface structures follow the cavity profile and thus a more complex alignment is formed.

At the same time, the laser processing debris that remained after ultrasonic cleaning were transferred to the replicas during the initial injection moulding cycles (see Fig. 8c). Therefore, it is a common practice to discard the initial moulded parts[41], and instead begin analysing the replicas when the injection moulding process can be considered stable and performing as intended. In this research, the replicated topographies and their functional characteristics were studied after the first 50 injection moulding shots.

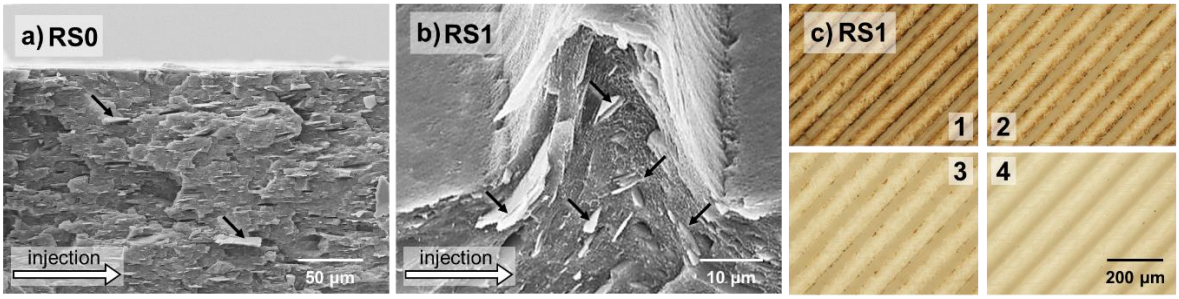

Figure 8. SEM views of fractured PP replicas along the flow direction of injection moulded samples with d) untextured (RS0) and e) Grooves (RS1) inserts. f) Optical images of the first four RS1 parts.

Notes: The images in e) and in the insets a) and b) were viewed at 45° angle and the black arrows point out some mineral fillers.

3.3 Effects of in-process mould wear on surface topographies

5000 replicas were produced using the 30 wt% talc-loaded polypropylene from each insert. The surfaces of the inserts were analysed before and after the 5000 injection moulding cycles. Inspections revealed that the laser processing debris were removed after the moulding cycles (also observed on the first moulded replicas, such as on Fig. 8c) and that some pits and scuffings were formed, despite the fact that the inserts were hardened. Such surface damages could be attributed to mould wear arising from shear and frictional forces occurring between the insert surface and the flow of the highly viscous molten polymer combined with fillers during the injection and demoulding stages[25,30,31]. The damages are mainly found on the surface of the inserts but not inside the micro-scale grooves or pillars, as shown for example on C1 on Fig. 9a. In particular, adhesive wear on inserts' surfaces induced the formation of pits of various sizes and can be explained as a combined effect of adhesive and corrosion wear. An example of underlying mechanism of pit formation, as shown in Fig. 9b, is the removal of any inclusions present on the surface of the inserts, followed by a corrosive damage of the exposed material. Moreover, it is worth mentioning that abrasive wear was not directly observed in this work. The scratches and plough marks seen on carburised inserts (such as on Fig. 9b) are due to the gentle post-polishing step after the plasma treatment, as described in Section 2.1. Traces of polypropylene could be found entrapped in the formed pits (see Fig. 9c). Overall, further research would be needed to understand the underlaying mechanism of the types of surface damages and their evolutions along the injection moulding cycles. Such surface damage or polymer entrapment could have detrimental effects on the functional response of replicated surfaces, and therefore should be minimised.

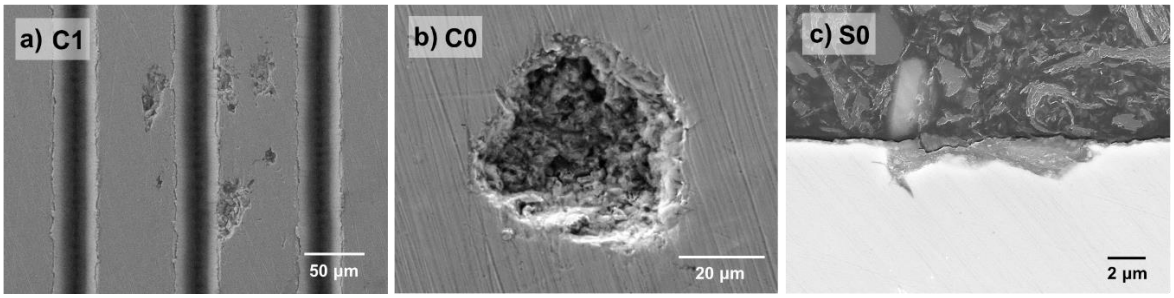

Figure 9. SEM micrographs of carburised inserts after 5000 injection cycles: a) C1 and b) C0. c) Cross section of a representative surface damage/wear on S0, exhibiting traces of PP.

Further inspections of the inserts revealed the presence of redeposited material along the grooves, on both carburised and untreated stainless steel as shown in Fig. 10a-b. Through a closer look at the side walls it is possible to distinguish LIPSS inside the grooves (see Fig. 10b). Therefore, following the injection cycles, the redeposited material found at the edge of the grooves was removed due to physical delamination and wear (see Fig. 10c-d). At the same time some micro cracks into the carburised layer had been initiated near the interface with the bulk material (see Fig. 10d). Such failure mode has been previously reported for laser-textured nitrided stainless steel[29] or plastic injection moulding[31], however, it is unlikely for carburised samples where the treated layer is usually much thicker and with a superior load bearing capacity.

Regarding the Lotus-leaf like structures, the redeposited material formed bulges around the holes, with no signs of any delamination (see Fig. 10e). The observed differences in comparison to the groove structures, can be attributed to the different laser processing

conditions or wear mechanisms present during the injection moulding cycles. Lastly, the submicron textures, especially LIPSS, were still visible after the 5000 injections, with approximate aspect ratios between 1:5 and 1:10 on both untreated and carburised stainless steel as shown in Fig. 10h-i.

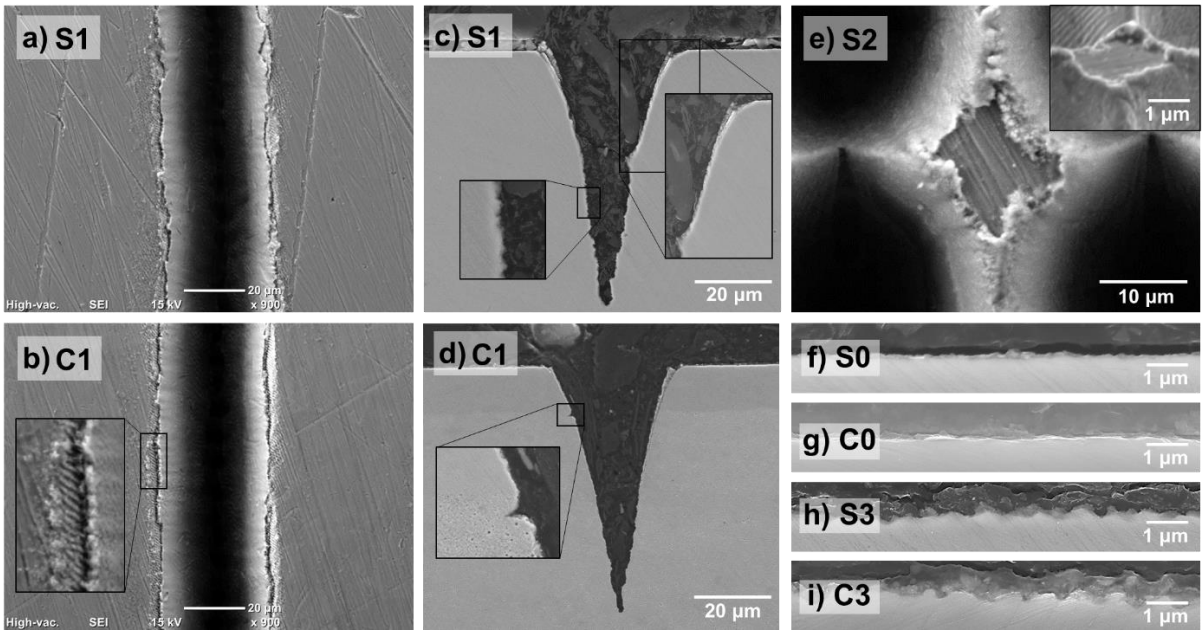

Figure 10. SEM top views and cross sections of the laser-textured inserts after 5000 injection moulding cycles: a,c) S1, b,d) C1, e) S2, f) S0, g) C0, h) S3, i) C3.

Note: the inset in e) was viewed at 45° angle.

As a result of abrasion and friction phenomena, the surface finish of the inserts was only slightly altered. Notably, the roughness of untreated inserts increased marginally after 5000 injection moulding cycles while it decreased slightly on the carburised ones. However, the S_a values remained of a similar magnitude, from 60 to 100 nm, with a maximum variation of + 3 % and - 10 % (see Fig. 11a). In comparison with other inserts a lower roughness variation was observed on the LIPSS surfaces. On the other two textured inserts, the depth of the grooves and the holes was almost the same after the 5000 moulding cycles while the peak-to-valley height of the laser textures varied up to - 12 % (see Fig. 11b) due to the removal of debris from the surface and, eventually, the general wear of the top surface.

The topography evolution of the PP replicas with the increase of injection moulding cycles was also analysed. Arithmetical mean roughness (S_a) and maximum peak-to-valley heights (Δ_z) were measured on LIPSS (see Fig. 11c,e) and groove (see Fig. 11d,f) structures after 50, 200, 500, 1000, 2000, 3000, 4000 and 5000 cycles. On LIPSS replicas the roughness varied in the range from 184 to 272 nm without any specific trends. However, the height of the grooves decreased after the first 100 cycles and then increased marginally from 31 to 34 µm on replicas from both untreated and carburised inserts. Overall, the standard deviation values of roughness were smaller on replicas produced with the carburised inserts and this can be attributed to their higher hardness and wear resistance.

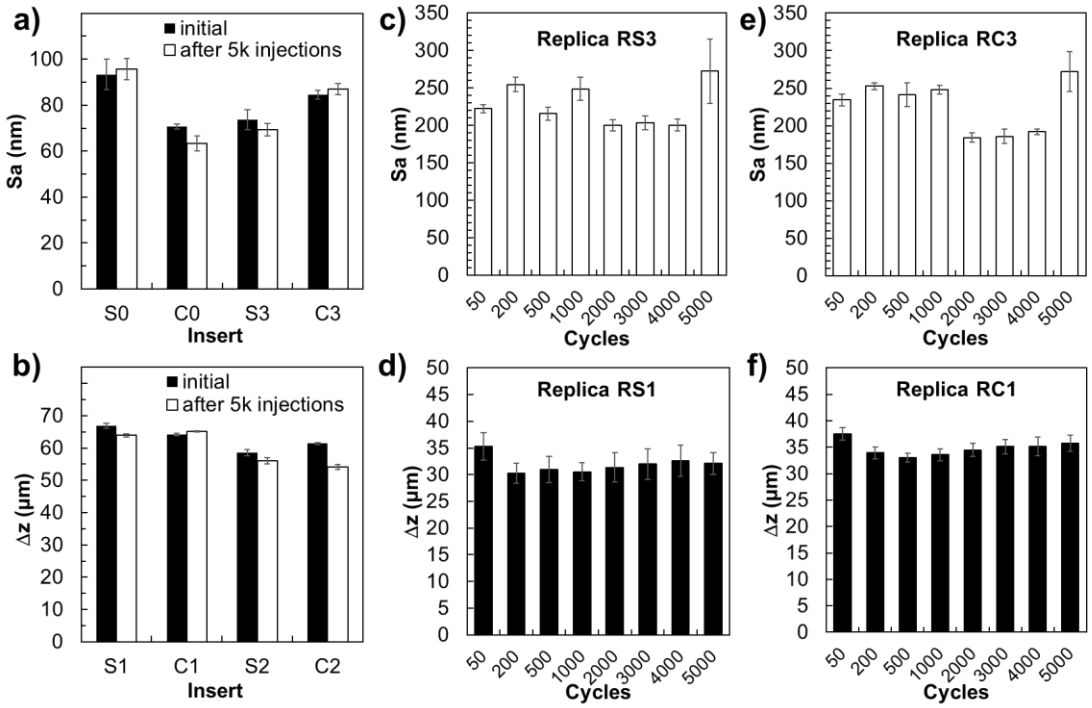

Figure 11. The evolution of surface roughness on inserts and replicas with the increase of injection moulding cycles. Arithmetical mean height measurements (top row) and maximum peak-to-valley heights (bottom row) obtained on inserts, i.e. a) S0, C0, S3, C3 and b) S1, C1, S2, C2; and PP replicas, i.e. c) RS3, d) RS1, e) RC3 and f) RC1.

The topographies of replicated grooves from both treated and untreated inserts were similar (see Fig. 12a-d). After 5000 injection moulding cycles, the walls were still covered with a submicron roughness and the top of the groove remained smooth, with sporadic talc platelets visible. However, micro-scale defects were apparent on replicated topographies, e.g. some portions of the grooves or the holes were missing, as shown in Fig. 12e-f. This can be explained with polymer or wear debris clogging the insert topographies. Regarding the LIPSS inserts, the submicron features seemed to have been damaged after the first 200 mouldings as shown in Fig. 12g. Such small replication defects can appear following wear damage on the inserts. After 5000 mouldings, damages such as scratches and wear tracks were much more apparent across the surfaces (see Fig. 12h). Additionally, the wear pits were replicated forming micro-scale bumps on the PP surfaces.

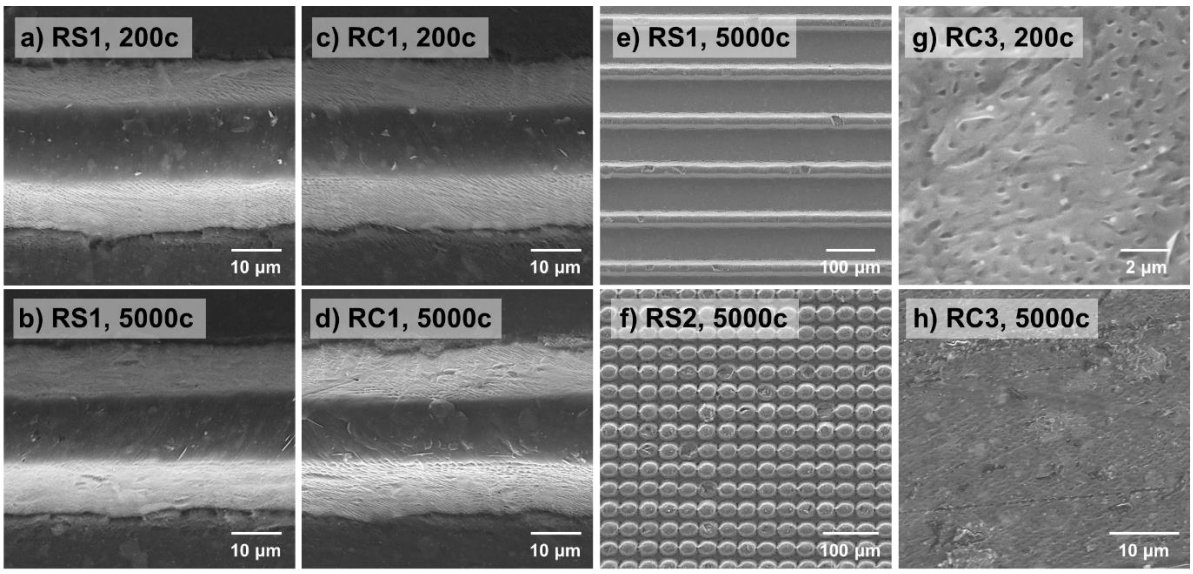

Figure 12. SEM top views of moulded PP samples: RS1 and RC1 surfaces, after 200 mouldings a) and c), and after 5000 mouldings b) and d), respectively. Magnified views of RS1 and RS2 surfaces after 5000 injections in e) and f), correspondingly. Defects on RC3 after 200 and 5000 mouldings in g) and h), respectively.

3.4 Effects of in-process wear on surface functionality

The replicated PP surfaces exhibited different wetting properties, ranging from hydrophobic to superhydrophobic as shown in Fig. 13a-b. The water contact angles measured on untextured PP samples (RS0, RC0) were between 105° and 110°. Single-scale submicron texturing (LIPSS) increased the initial contact angles to approximately 130° for RS3 and RC3. The PP replicas with grooves (RS1, RC1) and Lotus-leaf like (RS2, RC2) textures were superhydrophobic, initially, with contact angles of approximately 155° and low rolling-off angles.

Without surface texturing, the wetting properties were relatively stable even after 5000 cycles. However, the hydrophobicity of all investigated topographies was effected, especially decreased significantly with the increase of moulding cycles, as shown in Fig. 13b.

For the replicas with LIPSS textures, the decrease of contact angle was progressive from 132° to 114° with the increase of the moulding cycles and the spread of the measurements remained low, approximately +/- 4° (see Fig. 13c). Marginal changes were observed when using the carburised insert (see Fig. 13e). However, in some cases, sharp variations in contact angles were observed, presumably due to the presence of wear defects where the water drops would pin and spread.

Regarding dual micro/nano-scale textures, the contact angles decreased from more than 150° to approximately 125°, 140°, 135° and 140° on RS1, RC1, RS2 and RC2 samples, respectively. Overall, the PP replicas produced with the dual micro/nano-textured carburised inserts (RC1 and RC2) retained higher contact angles after 5000 mouldings (see Fig. 13b). This can be attributed to their higher hardness and wear resistance when replicating micro-textured surfaces with talc-loaded polymer compound. In particular, following the 5000 moulding cycles, the highest contact angle of almost 140° was obtained on the groove-textured PP replicas (RC1) produced with the carburised insert in comparison to the bigger CA decrease on other three surface topographies investigated in this research.

In case of the samples with the grooves (RS1 and RC1), it should also be noted that an average contact angle above 150° was maintained after 1000 and 3000 mouldings,

respectively (see Fig. 13d,f). This clearly demonstrated a three-fold increase in durability of the grooves' functional properties of the replicas produced with the plasma carburised inserts, i.e. their hydrophobicity, in comparisons to those produced with as-received steel inserts.

As reported by Wenzel, for a hydrophobic flat substrate, an increase of surface roughness leads to a higher hydrophobicity[8]. A further increase of surface roughness and area ratio could lead to even higher contact angles, sometimes above 150°, due to trapped air[9]. However, there was no apparent correlation between the roughness variations and the contact angles in this research. For untextured or submicron topographies, the roughness of LIPSS samples (RS3, RC3) did not significantly varied before and after the injection moulding cycles, but the contact angles decreased progressively. It is worth noting that the areal parametrers, S_a or Δ_z used in this research to study the surface topography evolution on replicas, were not affected by any localised damage on injection mouldings. Therefore, these areal parameters were selected to analyse the surface topography and not S_a and S_z that were used in another research to investigate dependences between surface roughness and superhydrophobicity on injection moulded parts[28], Thus, the use of S_a or Δ_z could explain the reduction of hydrophobicity with the development of surface defects and the increase of roughness values, as discussed in Section 3.2. Especially, any localised defects as a result of the mould wear may breach the quasi-static equilibrium of the droplet, spreading the liquid drop and thus decreasing the contact angle. Further research is necessary to determine the specific effects of mould wear on replicas with the increase of moulding cycles and also what areal parameters could be used to judge indirectly about the wetting properties of injection moulded parts.

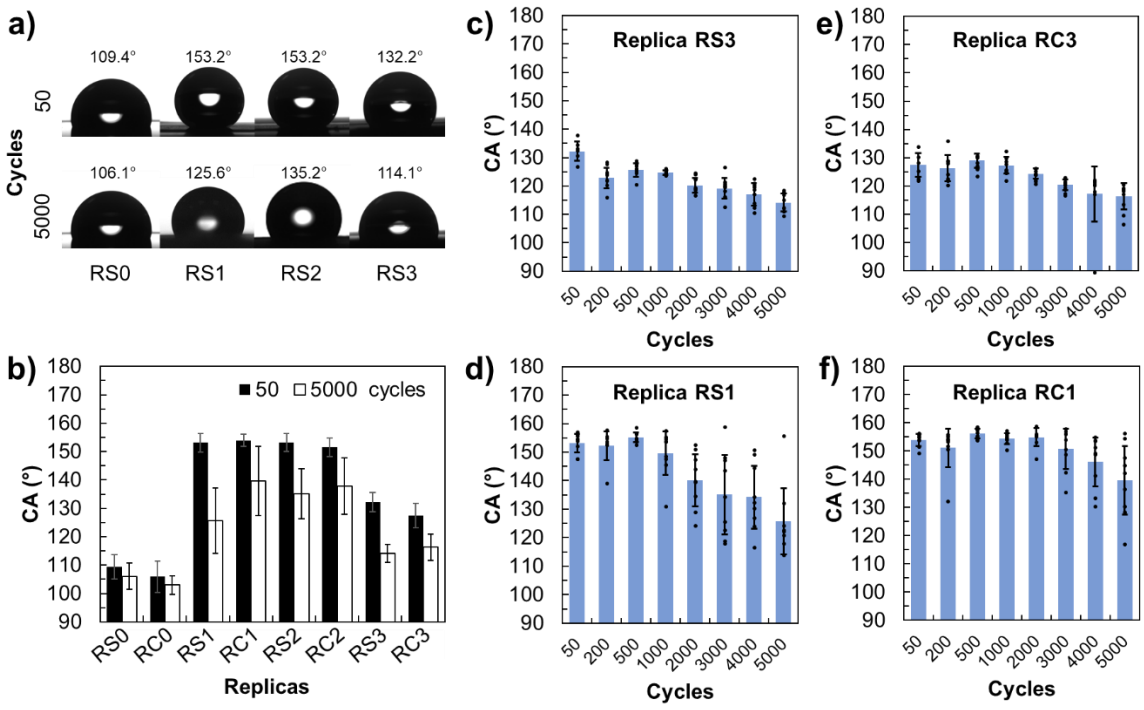

Figure 13. Wetting properties of textured PP replicas: a) 6 µl water drops on surfaces replicated using untreated stainless steel inserts after 50 and 5000 mouldings; b) comparison of contact angles obtained on replicas using all 8 inserts, after 50 and 5000 injection moulding cycles; and the evolution of contact angles on c) RS3, d) RS1, e) RC3 and f) RC1, after 50, 200, 500, 1000, 2000, 3000, 4000 and 5000 mouldings.

4. Conclusion

In this research, a process chain for replicating superhydrophobic thermoplastic surfaces was investigated. The process chain included, firstly low temperature plasma carburising of austenitic stainless steel to increase its hardness, followed by laser texturing to produce replication masters and finally thermoplastic replication through injection moulding. Ultrashort laser pulses were used to texture the surface of plasma treated inserts, by producing three different functional topographies: microscale grooves, holes and sub-microscale LIPSS. Then, a commercially available talc-loaded PP was used to fabricate 5000 moulded parts with the carburised laser-textured inserts. The surface structures on inserts were replicated on PP parts with an efficiency of approximately 55% and 70-80% for microscale and submicron textures, respectively. Replicas of submicron LIPSS led to an increase in water contact angle from 110 to 130°, while dual-scale topographies (micro-scale structures covered with LIPSS) exhibited superhydrophobic properties, i.e. water contact angles higher than 150° and low rolling-off angles.

The inspection of the inserts revealed that debris from the laser processing step were removed after initial injection moulding cycles and clear signs of wear and surface damages were observed after 5000 mouldings. Also, the carburised layer exhibited some cracks at the interface with the bulk material, which should be further investigated, especially its effects on mould durability.

The evolution of surface topographies with the increase of injection moulding cycles were analysed together with their wettability, both on inserts and replicas. Any wear or damage on inserts as a result of the increasing moulding cycles, were replicated onto the PP surfaces and had a clear impact on their topographies, i.e. arithmetical mean roughness (S_a) and maximum peak-to-valley heights (Δ_z). These two standardized areal parameters could be used to monitoring the level of wear defects and surface damages that impact the functional textures on replicas and thus indirectly the intended surface response on thermoplastic replicas.

Superhydrophobicity was retained on PP replicas for longer, approximately 3000 cycles, when the groove-structured carburised insert was used, whereas, only 1000 parts with similar wetting properties were produced with its respective untreated counterpart. Regarding the submicron LIPSS textures, the contact angles of replicas decreased after 5000 injections from 132° to 114°, close to the values obtained on untextured PP replica. In general, the PP replicas produced with the carburised inserts retained higher contact angles after 5000 cycles. This is a clear evidence of the plasma treatment beneficial effects on replication masters, especially on inserts' wear resistance and through this the wetting properties of textured thermoplastic replicas were retained for longer.

Acknowledgment

The research was carried out in the framework of the Laser4Fun project on "Short Pulsed Laser Micro/Nanostructuring of Surfaces for Improved Functional Applications" (Laser4Fun), which has received funding from the European Union's H2020 research and innovation programme under the Marie Skłodowska-Curie grant agreement No. 675063 (www.laser4fun.eu). The work was also supported by three other H2020 projects, i.e. "High-Impact Injection Moulding Platform for mass-production of 3D and/or large micro-structured surfaces with Antimicrobial, Self-cleaning, Anti-scratch, Anti-squeak and Aesthetic functionalities" (HIMALAIA, No. 766871), "Process Fingerprint for Zero-defect Net-shape Micromanufacturing" (MICROMAN, No. 674801) and "Modular laser based additive manufacturing platform for large scale industrial applications" (MAESTRO, No. 723826). Further support was provided by the UKIERI DST programme "Surface functionalisation for food, packaging, and healthcare applications". Finally, the authors would like to acknowledge

the support and assistance of the University of Bradford and BSH Electrodomésticos España, S.A. in conducting this research.

References

(1) Liu, K.; Yao, X.; Jiang, L. Recent Developments in Bio-Inspired Special Wettability. *Chem. Soc. Rev.* **2010**, *39* (8), 3240. https://doi.org/10.1039/b917112f.

(2) Müller, F. A.; Kunz, C.; Gräf, S. Bio-Inspired Functional Surfaces Based on Laser-Induced Periodic Surface Structures. *Materials* **2016**, *9* (6), 476. https://doi.org/10.3390/ma9060476.

(3) Yong, J.; Chen, F.; Yang, Q.; Jiang, Z.; Hou, X. A Review of Femtosecond-Laser-Induced Underwater Superoleophobic Surfaces. *Adv. Mater. Interfaces* **2018**, *5* (7), 1701370. https://doi.org/10.1002/admi.201701370.

(4) Zorba, V.; Stratakis, E.; Barberoglou, M.; Spanakis, E.; Tzanetakis, P.; Anastasiadis, S. H.; Fotakis, C. Biomimetic Artificial Surfaces Quantitatively Reproduce the Water Repellency of a Lotus Leaf. *Adv. Mater.* **2008**, *20* (21), 4049–4054. https://doi.org/10.1002/adma.200800651.

(5) Long, J.; Fan, P.; Gong, D.; Jiang, D.; Zhang, H.; Li, L.; Zhong, M. Superhydrophobic Surfaces Fabricated by Femtosecond Laser with Tunable Water Adhesion: From Lotus Leaf to Rose Petal. *ACS Appl. Mater. Interfaces* **2015**, *7* (18), 9858–9865. https://doi.org/10.1021/acsami.5b01870.

(6) Helbig, R.; Nickerl, J.; Neinhuis, C.; Werner, C. Smart Skin Patterns Protect Springtails. *PLOS ONE* **2011**, *6* (9), e25105. https://doi.org/10.1371/journal.pone.0025105.

(7) Romano, J.-M.; Helbig, R.; Fraggelakis, F.; Garcia-Giron, A.; Werner, C.; Kling, R.; Dimov, S. Springtail-Inspired Triangular Laser-Induced Surface Textures on Metals Using MHz Ultrashort Pulses. *J. Micro Nano-Manuf.* **2019**, *7* (2), 024504. https://doi.org/10.1115/1.4043417.

(8) Wenzel, R. N. Resistance of Solid Surfaces to Wetting by Water. *Ind. Eng. Chem.* **1936**, *28* (8), 988–994. https://doi.org/10.1021/ie50320a024.

(9) Cassie, A. B. D.; Baxter, S. Wettability of Porous Surfaces. *Trans. Faraday Soc.* **1944**, *40* (0), 546–551. https://doi.org/10.1039/TF9444000546.

(10) Koch, K.; Bhushan, B.; Jung, Y. C.; Barthlott, W. Fabrication of Artificial Lotus Leaves and Significance of Hierarchical Structure for Superhydrophobicity and Low Adhesion. *Soft Matter* **2009**, *5* (7), 1386–1393. https://doi.org/10.1039/B818940D.

(11) Kietzig, A.-M.; Mirvakili, M. N.; Kamal, S.; Englezos, P.; Hatzikiriakos, S. G. Laser-Patterned Super-Hydrophobic Pure Metallic Substrates: Cassie to Wenzel Wetting Transitions. *J. Adhes. Sci. Technol.* **2011**, *25* (20), 2789–2809. https://doi.org/10.1163/016942410X549988.

(12) Busà, C.; Stanley Rickard, J. J.; Chun, E.; Chong, Y.; Navaratnam, V.; Oppenheimer, P. G. Tunable Superapolar Lotus-to-Rose Hierarchical Nanosurfaces via Vertical Carbon Nanotubes Driven Electrohydrodynamic Lithography. *Nanoscale* **2017**, *9* (4), 1625–1636. https://doi.org/10.1039/C6NR08706J.

(13) Cai, Y.; Chang, W.; Luo, X.; Sousa, A. M. L.; Lau, K. H. A.; Qin, Y. Superhydrophobic Structures on 316L Stainless Steel Surfaces Machined by Nanosecond Pulsed Laser. *Precis. Eng.* **2018**, *52*, 266–275. https://doi.org/10.1016/j.precisioneng.2018.01.004.

(14) Fraggelakis, F.; Mincuzzi, G.; Lopez, J.; Manek-Hönninger, I.; Kling, R. Texturing Metal Surface with MHz Ultra-Short Laser Pulses. *Opt. Express* **2017**, *25* (15), 18131–18139. https://doi.org/10.1364/OE.25.018131.

(15) Kietzig, A.-M.; Hatzikiriakos, S. G.; Englezos, P. Patterned Superhydrophobic Metallic Surfaces. *Langmuir* **2009**, *25* (8), 4821–4827. https://doi.org/10.1021/la8037582.

(16) Wu, B.; Zhou, M.; Li, J.; Ye, X.; Li, G.; Cai, L. Superhydrophobic Surfaces Fabricated by Microstructuring of Stainless Steel Using a Femtosecond Laser. *Appl. Surf. Sci.* **2009**, *256* (1), 61–66. https://doi.org/10.1016/j.apsusc.2009.07.061.

(17) Martínez-Calderon, M.; Rodríguez, A.; Dias-Ponte, A.; Morant-Miñana, M. C.; Gómez-Aranzadi, M.; Olaizola, S. M. Femtosecond Laser Fabrication of Highly Hydrophobic Stainless Steel Surface with Hierarchical Structures Fabricated by Combining Ordered Microstructures and LIPSS. *Appl. Surf. Sci.* **2016**, *374*, 81–89. https://doi.org/10.1016/j.apsusc.2015.09.261.

(18) Vorobyev, A. Y.; Guo, C. Direct Femtosecond Laser Surface Nano/Microstructuring and Its Applications. *Laser Photonics Rev.* **2013**, *7* (3), 385–407. https://doi.org/10.1002/lpor.201200017.
(19) Huerta-Murillo, D.; García-Girón, A.; Romano, J. M.; Cardoso, J. T.; Cordovilla, F.; Walker, M.; Dimov, S. S.; Ocaña, J. L. Wettability Modification of Laser-Fabricated Hierarchical Surface Structures in Ti-6Al-4V Titanium Alloy. *Appl. Surf. Sci.* **2019**, *463*, 838–846. https://doi.org/10.1016/j.apsusc.2018.09.012.
(20) Rebollar, E.; Aldana, J. R. V. de; Martín-Fabiani, I.; Hernández, M.; Rueda, D. R.; Ezquerra, T. A.; Domingo, C.; Moreno, P.; Castillejo, M. Assessment of Femtosecond Laser Induced Periodic Surface Structures on Polymer Films. *Phys. Chem. Chem. Phys.* **2013**, *15* (27), 11287–11298. https://doi.org/10.1039/C3CP51523K.
(21) Mezera, M.; van Drongelen, M.; Römer, G. R. B. E. Laser-Induced Periodic Surface Structures (LIPSS) on Polymers Processed with Picosecond Laser Pulses. *J. Laser Micro Nanoeng.* **2018**, *13* (2), 105–116. http://dx.doi.org/10.2961/jlmn.2018.02.0010.
(22) Cardoso, M. R.; Martins, R. J.; Dev, A.; Voss, T.; Mendonca, C. R. Highly Hydrophobic Hierarchical Nanomicro Roughness Polymer Surface Created by Stamping and Laser Micromachining. *J. Appl. Polym. Sci.* **2015**, *132* (24), n/a-n/a. https://doi.org/10.1002/app.42082.
(23) Jiang, D.; Fan, P.; Gong, D.; Long, J.; Zhang, H.; Zhong, M. High-Temperature Imprinting and Superhydrophobicity of Micro/Nano Surface Structures on Metals Using Molds Fabricated by Ultrafast Laser Ablation. *J. Mater. Process. Technol.* **2016**, *236*, 56–63. https://doi.org/10.1016/j.jmatprotec.2016.05.009.
(24) Rajab, F. H.; Liu, Z.; Wang, T.; Li, L. Controlling Bacteria Retention on Polymer via Replication of Laser Micro/Nano Textured Metal Mould. *Opt. Laser Technol.* **2019**, *111*, 530–536. https://doi.org/10.1016/j.optlastec.2018.10.031.
(25) Brezinová, J.; Guzanová, A. Friction Conditions during the Wear of Injection Mold Functional Parts in Contact with Polymer Composites. *J. Reinf. Plast. Compos.* **2010**, *29* (11), 1712–1726. https://doi.org/10.1177/0731684409341675.
(26) Lapcik, L.; Jindrova, P.; Lapcikova, B.; Tamblyn, R.; Greenwood, R.; Rowson, N. Effect of the Talc Filler Content on the Mechanical Properties of Polypropylene Composites. *J. Appl. Polym. Sci.* **2008**, *110* (5), 2742–2747. https://doi.org/10.1002/app.28797.
(27) Han, J.; Cai, M.; Lin, Y.; Liu, W.; Luo, X.; Zhang, H.; Wang, K.; Zhong, M. Comprehensively Durable Superhydrophobic Metallic Hierarchical Surfaces via Tunable Micro-Cone Design to Protect Functional Nanostructures. *RSC Adv.* **2018**, *8* (12), 6733–6744. https://doi.org/10.1039/C7RA13496G.
(28) Romano, J.-M.; Gulcur, M.; Garcia-Giron, A.; Martinez-Solanas, E.; Whiteside, B. R.; Dimov, S. S. Mechanical Durability of Hydrophobic Surfaces Fabricated by Injection Moulding of Laser-Induced Textures. *Appl. Surf. Sci.* **2019**, *476*, 850–860. https://doi.org/10.1016/j.apsusc.2019.01.162.
(29) Garcia-Giron, A.; Romano, J. M.; Liang, Y.; Dashtbozorg, B.; Dong, H.; Penchev, P.; Dimov, S. S. Combined Surface Hardening and Laser Patterning Approach for Functionalising Stainless Steel Surfaces. *Appl. Surf. Sci.* **2018**, *439*, 516–524. https://doi.org/10.1016/j.apsusc.2018.01.012.
(30) Bienk, E. J.; Mikkelsen, N. J. Application of Advanced Surface Treatment Technologies in the Modern Plastics Moulding Industry. *Wear* **1997**, *207* (1), 6–9. https://doi.org/10.1016/S0043-1648(96)07503-5.
(31) Crema, L.; Lucchetta, G. A Study of Mold Friction and Wear in Injection Molding of Plastic-Bonded Hard Ferrite. *Key Eng. Mater.* **2014**, *611–612*, 460–472. https://doi.org/10.4028/www.scientific.net/KEM.611-612.460.
(32) Dong, H. S-Phase Surface Engineering of Fe-Cr, Co-Cr and Ni-Cr Alloys. *Int. Mater. Rev.* **2010**, *55* (2), 65–98. https://doi.org/10.1179/095066009X12572530170589.
(33) Gualtieri, E.; Borghi, A.; Calabri, L.; Pugno, N.; Valeri, S. Increasing Nanohardness and Reducing Friction of Nitride Steel by Laser Surface Texturing. *Tribol. Int.* **2009**, *42* (5), 699–705. https://doi.org/10.1016/j.triboint.2008.09.008.
(34) Byskov-Nielsen, J.; Savolainen, J.-M.; Christensen, M. S.; Balling, P. Ultra-Short Pulse Laser Ablation of Copper, Silver and Tungsten: Experimental Data and Two-Temperature Model Simulations. *Appl. Phys. A* **2011**, *103* (2), 447–453. https://doi.org/10.1007/s00339-011-6363-7.
(35) Bonse, J.; Rosenfeld, A.; Krüger, J. On the Role of Surface Plasmon Polaritons in the Formation of Laser-Induced Periodic Surface Structures upon Irradiation of Silicon by Femtosecond-Laser Pulses. *J. Appl. Phys.* **2009**, *106* (10), 104910. https://doi.org/10.1063/1.3261734.

(36) Huang, M.; Zhao, F.; Cheng, Y.; Xu, N.; Xu, Z. Origin of Laser-Induced Near-Subwavelength Ripples: Interference between Surface Plasmons and Incident Laser. *ACS Nano* **2009**, *3* (12), 4062–4070. https://doi.org/10.1021/nn900654v.
(37) Yasumaru, N.; Sentoku, E.; Miyazaki, K.; Kiuchi, J. Femtosecond-Laser-Induced Nanostructure Formed on Nitrided Stainless Steel. *Appl. Surf. Sci.* **2013**, *264*, 611–615. https://doi.org/10.1016/j.apsusc.2012.10.076.
(38) Romano, J.-M.; Garcia-Giron, A.; Penchev, P.; Dimov, S. Triangular Laser-Induced Submicron Textures for Functionalising Stainless Steel Surfaces. *Appl. Surf. Sci.* **2018**, *440*, 162–169. https://doi.org/10.1016/j.apsusc.2018.01.086.
(39) Patcharaphun, S.; Mennig, G. Prediction of Tensile Strength for Sandwich Injection Molded Short-Glass-Fiber Reinforced Thermoplastics. *J. Met. Mater. Miner.* **2007**, *17* (2), 9–16.
(40) Bay, R. S.; Tucker, C. L. Fiber Orientation in Simple Injection Moldings. Part I: Theory and Numerical Methods. *Polym. Compos.* **1992**, *13* (4), 317–331. https://doi.org/10.1002/pc.750130409.
(41) Baruffi, F.; Calaon, M.; Tosello, G. Micro-Injection Moulding In-Line Quality Assurance Based on Product and Process Fingerprints. *Micromachines* **2018**, *9* (6), 293. https://doi.org/10.3390/mi9060293.